

Developmental Changes in the Membrane Current Pattern, K⁺ Buffer Capacity, and Morphology of Glial Cells in the Corpus Callosum Slice

T. Berger,¹ J. Schnitzer,² and H. Kettenmann¹

¹Department of Neurobiology, University of Heidelberg, 6900 Heidelberg, Germany and ²Department of Neuroanatomy, Max Planck Institute for Brain Research, 6000 Frankfurt am Main 71, Germany

Recent studies indicated that glial cells in tissue culture can express a variety of different voltage-gated channels, while little is known about the presence of such channels in glial cells *in vivo*. We used a mouse corpus callosum slice preparation, in which after postnatal day 5 (P5) more than 99% of all perikarya belong to glial cells (Sturrock, 1976), to study the current patterns of glial cells during their development *in situ*. We combined the patch-clamp technique with intracellular labeling using Lucifer yellow (LY) and subsequent ultrastructural characterization. In slices of mice from P6 to P8, we predominantly found cells expressing delayed-rectifier K⁺ currents. They were similar to those described for cultured glial precursor cells (Sontheimer et al., 1989). A-type K⁺ currents or Na⁺ currents were not or only rarely observed, in contrast to cultured glial precursors. LY labeling revealed that numerous thin processes extended radially from the perikaryon of these cells, and ultrastructural observations suggested that they resemble immature glial cells. In slices of older mice (P10–13), when myelination of the corpus callosum has already commenced, many cells were characterized by an almost linear current–voltage relationship. This current pattern was similar to cultured oligodendrocytes (Sontheimer et al., 1989). Most processes of LY-filled cells with such a current profile extended parallel to each other. Electron microscopy showed that these processes surround thick, unmyelinated axons. We suggest that cells with oligodendrocyte-type electrophysiology are promyelinating oligodendrocytes. In contrast to cultured oligodendrocytes, membrane currents of promyelinating oligodendrocytes in the slice decayed during the voltage command. This decay was due not to inactivation, but to a marked change in the potassium equilibrium potential within the voltage jump. This implies that, in the more mature corpus callosum, small membrane polarizations in a physiological range can lead to extensive changes in the K⁺ gradient across the glial membrane within a few milliseconds.

Cultured glial cells express a variety of different ion channels and thus can no longer be regarded as electrically passive elements of the nervous system. Na⁺ channels, Ca²⁺ channels, and different types of K⁺ channels are found (for review, see Barres et al., 1990). While such studies in culture have greatly advanced our knowledge on the biophysical properties of these channels, they have added little to our understanding of their functional role. Glial channels are speculated to play a role in the control of ion homeostasis (Orkand et al., 1966; Newman, 1986) or proliferation (Chiu and Wilson, 1989). To establish more clearly their functional roles, these channels need to be studied in their natural environment, namely, in intact brain tissue.

Recently, Edwards et al. (1989) have succeeded in applying the patch-clamp technique to brain slices and were able to record whole-cell and single-channel currents from neurons *in situ*. In the present study, we have adopted this approach to a slice preparation of the mouse corpus callosum. In this part of the CNS, at 5 d postnatally more than 99% of all somata are thought to be of glial origin (Sturrock, 1976). In contrast to other parts of the CNS of mice, the corpus callosum “matures” relatively late. Five days after birth, only immature glial cells are detectable; myelination commences 11 d after birth and continues during the following 8 months (Sturrock, 1980).

The corpus callosum could thus serve as a model to address the following questions: What kind of voltage-gated currents do glial cells express *in situ*? Can currents be detected that are similar to those expressed by cortical oligodendrocytes *in vitro*? Is it possible to demonstrate that a developmental regulation of currents takes place in glial cells *in situ* that has been shown so far only for *in vitro* glial cells (Sontheimer et al., 1989)?

Therefore, we recorded membrane currents from glial cells in corpus callosum slices obtained from postnatal mice. These glial cells express voltage-gated channels that resemble in part those expressed *in vitro*; that is, their expression is developmentally regulated. In addition, we can correlate these electrophysiological changes to structural changes of these cells.

Materials and Methods

Preparation of brain slices and electrophysiological setup. Young mice [postnatal days 6–13 (P6–13)] were killed by decapitation, and their brains were dissected out. The forebrain hemispheres were cut into 150 μ m-thick slices in frontal orientation using a vibratome (FTB, Plano, Marburg, Germany). The corpus callosum was cut parallel to its axonal fascicles (Fig. 1). Slices were placed in a recording chamber at about 25°C mounted on the stage of a Zeiss microscope and fixed in the chamber using a U-shaped platinum wire with a grid of nylon threads (Edwards et al., 1989). The chamber was continuously perfused with a salt solution, and substances were added by changing the perfusate. Cell somata in the corpus callosum were visible in normal water-immersion optics and could be approached by the patch electrode.

Received Dec. 17, 1990; revised Apr. 8, 1991; accepted Apr. 12, 1991.

This work was supported by the Bundesministerium für Forschung und Technologie, the Hermann und Lilly Schilling-Stiftung, Boehringer-Ingelheim-Fonds (Stipendium to T.B.), the Max Planck Gesellschaft, and the Deutsche Forschungsgemeinschaft (Heisenberg-Stipendium SFB 317 to H.K.). We thank Drs. F. Edwards, A. Konnerth, and P. Stern for helpful comments during the work, W. Hofer and G.-S. Nam for excellent technical assistance, and C. Zieger for preparing the micrographs.

Correspondence should be addressed to Helmut Kettenmann, Institute of Neurobiology, University of Heidelberg, Im Neuenheimer Feld 345, D-6900 Heidelberg, Germany.

Copyright © 1991 Society for Neuroscience 0270-6474/91/113008-17\$05.00/0

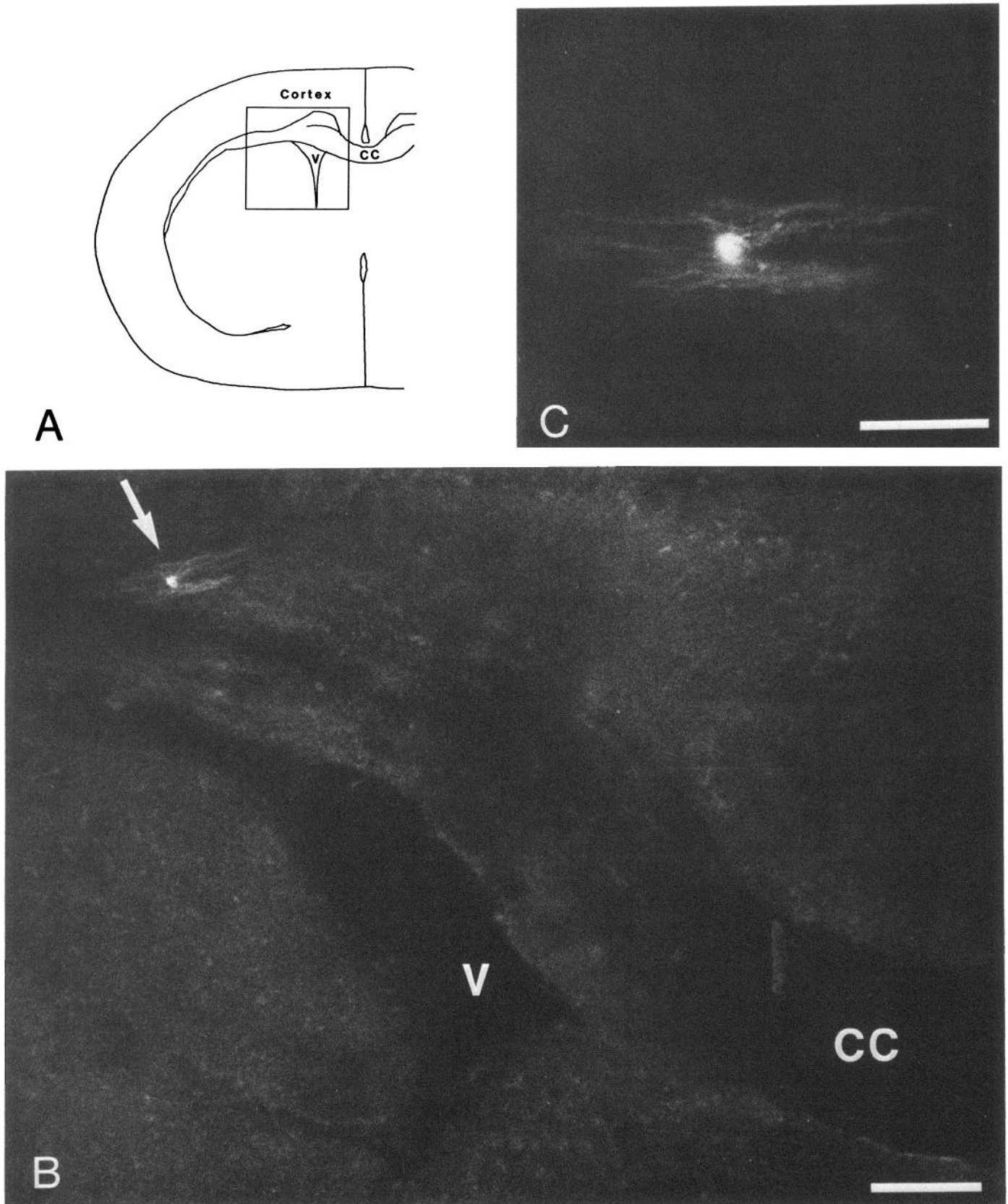


Figure 1. The preparation. *A*, Schematic drawing of the slice preparation used in this study: frontal section through the mouse brain at the level of the corpus callosum (CC; *V*, ventricle). The boxed area indicates the area of the slice seen in *B*. *B*, Slice of a P10 mouse brain. The arrow points to an LY-filled glial cell located in the corpus callosum. *C*, Higher magnification of the same LY-filled glial cell. Scale bars: *B*, 50 μm ; *C*, 25 μm .

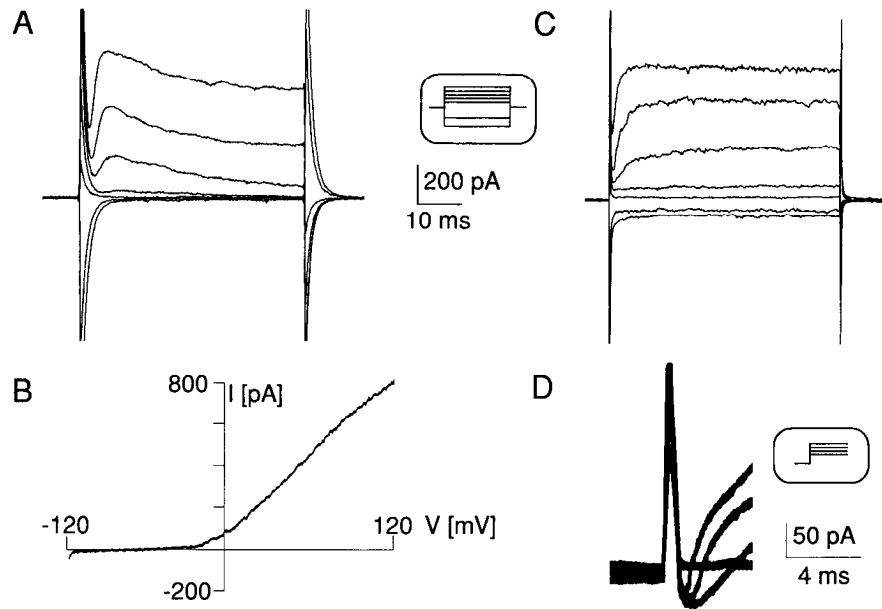


Figure 2. Currents from cells of P6–8. *A*, A cell in a corpus callosum slice from a P8 mouse was clamped from a holding potential of -70 mV to increasing de- and hyperpolarizing potentials (voltage pattern, see *inset*). The current responses for potential jumps to -160 , -120 , -60 , -40 , -20 , 0 , and 20 mV are shown. While hyperpolarizing pulses did not activate currents of significant amplitude, voltage- and time-dependent currents with slow activation were recorded with membrane depolarization. The current decayed with a time constant of 15 msec. In this figure, and in the following ones, leakage and capacitance currents were not subtracted. *B*, The steady state current (I) to voltage (V) relation was determined by a rampwise change of the holding potential from -120 to 120 mV (duration 1 sec), which induced a marked outward rectifying current response. *C*, A similar recording as described in *A* was obtained from another cell in a slice from a P6 mouse. In response to depolarizing pulses, a voltage- and time-dependent outward current without inactivation was observed. *D*, Transient inward currents were activated after jumps to -20 , -10 , 0 , and $+10$ mV from a holding potential of -70 mV (voltage pattern, see *inset*) in a cell from a slice from a P7 mouse. A jump to 0 mV elicited the largest inward current.

Cells with a rounded and pale appearance located near the surface of the slice were not selected for recording, while cells having a clear, dark membrane surface and lying around 30 μm deep in the tissue were analyzed. In contrast to the method described by Edwards et al. (1989), a separate pipette was not used to blow off cellular debris, as axonal bundles could not be removed. Instead, positive pressure was applied to the pipette while it was lowered under microscopic control. The axonal bundles were blown aside, and the pipette tip could be placed onto the surface of a cell soma.

Membrane currents were measured with the patch-clamp technique in the whole-cell recording configuration (Hamill et al., 1981). Current signals were amplified with conventional electronics (EPC-7 amplifier, List Electronics, Darmstadt, Germany), filtered at 3 kHz, and sampled at 5 kHz by an interface connected to an AT-compatible computer system, which also served as a stimulus generator.

Solutions and electrodes. The standard bathing solution contained (in mM) NaCl, 150 ; KCl, 5.4 ; CaCl_2 , 2 ; MgCl_2 , 1 ; HEPES, 5 ; and glucose, 10 . The pH was adjusted with NaOH to 7.2 , and the solution was gassed with O_2 . In some experiments, 10 mM NaCl was replaced by an equimolar amount of BaCl_2 to block potassium currents. Recording pipettes were fabricated from borosilicate capillaries (Hilgenberg, Malsfeld, Germany), with resistances ranging from 3 to 5 $\text{M}\Omega$, coated with Sigmacote (Sigma). The pipette contained (in mM) KCl, 130 ; CaCl_2 , 0.5 ; EGTA, 5 ; MgCl_2 , 2 ; HEPES, 10 ; ATP, 3 ; and GTP, 0.4 . Ca^{2+} activity was calculated to be approximately 11 nM. The pH was adjusted with NaOH to 7.2 . The pipette always contained 1 mg/ml Lucifer yellow (LY).

Intracellular staining of cells. During recording, cells were filled with LY by dialyzing the cytoplasm with the patch pipette solution. To avoid destruction of the cell as the pipette was pulled off after recording, the seal was destroyed by a large hyperpolarizing current injection. Following recording, slices were fixed for 3 – 5 hr at room temperature in 4% paraformaldehyde, 0.25% glutaraldehyde in 0.1 M phosphate buffer, pH 7.2 . Slices were then transferred to phosphate buffer. LY-filled cells were examined in a microscope equipped with the appropriate filter combination (BP 400–440, FT 460, LP 470).

Electron microscopy. For electron microscopic observation, LY fluorescence was replaced during a photooxidative process by an electron-

dense 3,3'-diaminobenzidine (DAB) reaction product. The method followed closely that described by Maranto (1982) with the modifications reported by Sandell and Masland (1988). Slices were rinsed in 0.1 M Tris buffer (pH 8.2), placed on a microscopic slide, and incubated in a DAB solution (1.5 mg DAB/ml Tris buffer, supplemented with 1.0 mg potassium cyanide/ml to reduce background labeling). The injected cells were illuminated for about 15 min on a microscope stage using a $25\times$ objective and blue light (BP 400–440). Thus, it was possible to observe the fading of the LY and the formation of the brown DAB reaction product. The tissue was rinsed in Tris buffer and transferred to phosphate buffer, then to 0.1 M cacodylate buffer, pH 7.4 . Slices were post-fixed in 2% glutaraldehyde in cacodylate buffer for 2 hr. Small pieces of the slices containing the labeled cells were osmicated (2% osmium tetroxide in cacodylate buffer), dehydrated, flat embedded in Epon, and polymerized. The region containing the labeled cell was mounted on prepolymerized Epon blocks. Horizontal semithin (1 μm thick) sections were cut parallel to the axon fascicles and mounted on glass slides. As soon as the first traces of the DAB reaction product were detected, a series of ultrathin sections alternating with a semithin section was prepared. Ultrathin sections were stained with lead citrate and examined with an electron microscope (Zeiss EM 10).

Results

We investigated glial cells in frontal brain slices of the corpus callosum from mice between P6 and P13. Using water-immersion optics, cell somata located in the corpus callosum were readily recognized and could thus be approached by patch-clamp electrodes. After establishment of the whole-cell recording mode, the cell was dialyzed and thereby filled with LY. This enabled us to visualize the morphological appearance of the cells and simultaneously record the membrane currents. Figure 1 illustrates the location and shape of a LY-filled glial cell in the corpus callosum of a P10 mouse; this cell revealed electrophysiological

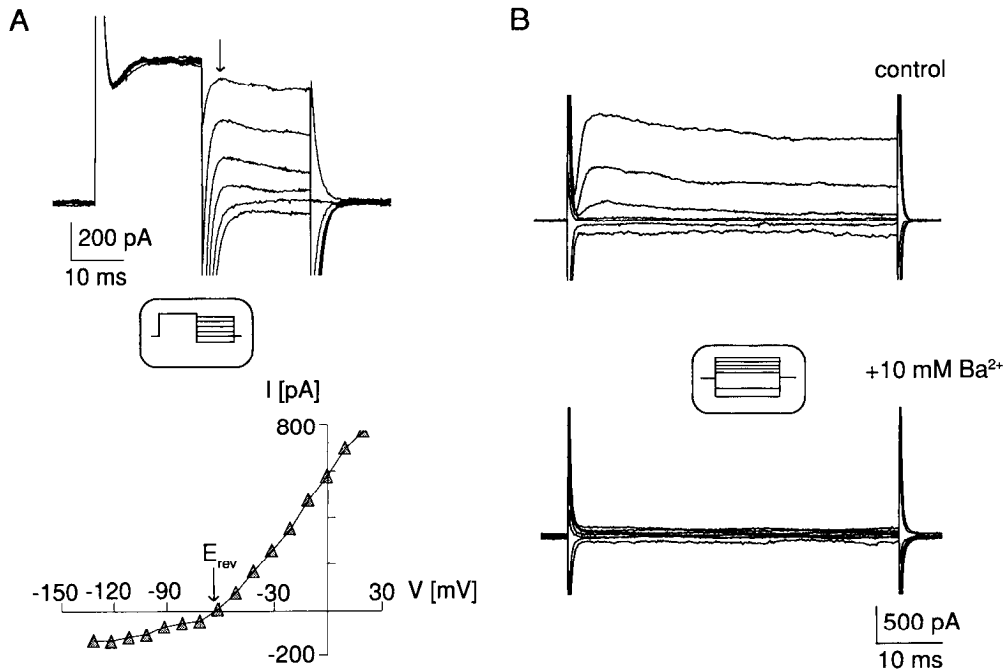


Figure 3. Identification of K⁺ currents from cells of P6–8. *A*, A tail current protocol was used to determine the reversal potential of the delayed outward current from a cell in a slice from a P6 mouse. In the *upper traces*, currents were activated with a voltage step from the holding potential to 20 mV. After 20 msec, the voltage command was switched to a series of more negative potentials (voltage pattern, see *inset*), and the family of current traces was superimposed. The current amplitude at the time marked by the *arrow* was determined and plotted in the *lower graph* as a function of the membrane potential. The reversal potential (E_{rev}) of the current was at -62 mV. *B*, Currents were activated as described for Figure 2*A* from a cell in a slice from a P6 mouse. Control currents (*upper family of traces*) were compared to those in the presence of 10 mM Ba²⁺ in the bath (*lower family of traces*). The almost complete blockade of currents in the presence of Ba²⁺ indicated that the current was carried by K⁺.

and morphological properties of an oligodendrocyte (for details, see below). Dye coupling was never observed, either in cells from P6–8 mice or in those from P10–13 mice. After replacing LY fluorescence by an electron-dense product, we could obtain ultrastructural details of the same cell and its environment. Subsequently, the properties of the membrane currents are the morphological features of the cells described.

Membrane currents of cells from P6 to P8

We recorded membrane currents from 46 cells in slices from P6–8 mice. The entrance potential after establishing the whole-cell mode averaged -54 mV (range, -31 to -77 mV; $N = 41$). Applying a standardized pulse protocol, the membrane potential was held at -70 mV and jumped for 50 msec to increasingly de- or hyperpolarizing potentials ranging from 20 to -160 mV. We could distinguish between three types of cells showing a distinct current pattern upon depolarization. One type was characterized by strongly outward rectifying currents (69%); another, by large inward currents (11%). In the third group of cells, no time- and voltage-dependent currents were recorded (20%).

The majority of cells showed a characteristic pattern of membrane currents: Depolarizing voltage steps activated an outward current that decayed during the voltage step ($N = 26$; Fig. 2*A*). The peak current for a voltage jump to 20 mV averaged 632 pA (range, 148–1457 pA; $N = 26$) after 5.9 msec (range, 3.3–10.5 msec; $N = 26$). The peak conductance had a mean of 6.32 nS. The steady state current component extrapolated from the fit of the current decay was 71% of the peak in cells exhibiting decay (450 pA; range, 39–1132 pA; $N = 26$). The current decay was fit in a time range between 5 and 25 msec after the start of the voltage command by a single exponential, yielding a mean time constant of 19 msec (range, 8–42 msec; $N = 21$) for a voltage jump to 20 mV. With hyperpolarizing voltage jumps, only minute, passive currents were observed, most likely reflecting leakage currents. The strongly outward rectifying behavior of the membrane currents is also reflected in the steady

state current–voltage relation obtained with voltage ramps ranging from -120 to 120 mV (1 sec duration; Fig. 2*B*).

In six cells, an outward rectifying current pattern with no decay was observed (Fig. 2*C*). The current peaked after 6.2 msec (range, 4.2–9.2 msec; $N = 4$) with an average amplitude of 544 pA (range, 216–755 pA; $N = 4$).

To determine the ionic specificity of the outward current, the current reversal potential was determined using a tail current protocol (Hille, 1984). The membrane was clamped to 20 mV to activate the outward current and consecutively clamped to less depolarized values ranging from 10 to -130 mV. The current amplitude was determined 2 msec after the voltage jump and reversed at about -60 mV, close to the potassium equilibrium potential ($E_{K^+} = -80$ mV; Fig. 3*A*). Application of Ba²⁺, which is known to block K⁺ channels, also significantly reduced the outward current ($N = 2$; to 6% and 15% of the control value, respectively; Fig. 3*B*). This blockade could not be reversed within the remaining recording time of up to 12 min.

We tested for the presence of A-type K⁺ currents by applying the standard pulse protocol for the isolation of this current type (Connor and Stevens, 1971). Therefore, the membrane potential was clamped to increasingly depolarized values, starting from two different holding potentials, -110 mV and -70 mV, respectively. Subtracting these two families of current traces did not reveal an additional current component selectively activated by jumping from the more negative holding potential. We thus could not detect A-type K⁺ currents in these cells.

In two of the cells described above, a transient inward current was observed that activated with depolarizing voltage jumps. This inward current had a peak amplitude of 83 and 240 pA, respectively, and kinetics similar to voltage-activated Na⁺ currents (Fig. 2*D*). In the current-clamp mode, cells were depolarized by a brief current pulse (90 pA) to test the capacity of the cell to generate action potentials. No action potentials could be detected.

The second group of cells observed in P6–8 corpus callosum

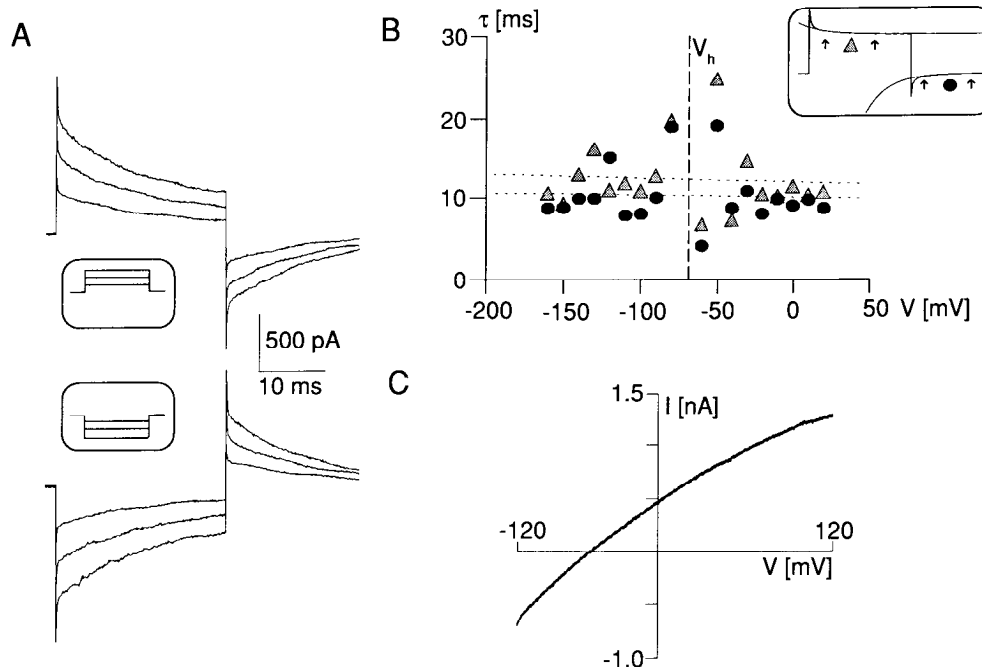


Figure 4. Currents from cells of P10–13. *A*, The voltage-clamp protocol described for Figure 2*A* was applied to a cell in a slice from a P10 mouse. The upper family of traces illustrates the current responses to a series of depolarizing voltage steps to -40 , -10 , and 20 mV from a holding potential of -70 mV; the lower family of responses, to hyperpolarizing voltage steps to -100 , -130 , and -160 mV. Note that an inward current is activated after switching from the depolarized potentials to the holding potential, and that an outward current is activated after switching from the hyperpolarized potentials. *B*, The time constant of the current decay was analyzed by monoexponentially fitting current traces of 25 msec duration starting 5 msec after a voltage step (analyzed time is indicated by arrows in the inset). Current traces after a voltage step from the holding potential to de- or hyperpolarized values (triangles) were compared to those for which the membrane potential was clamped back to the holding potential (circles) from the de- or hyperpolarized values. The time constants were plotted as a function of the de- or hyperpolarized potentials imposed during (triangles) or prior to the analyzed traces (circles). The time constants were not significantly different, and the means are denoted as horizontal dotted lines for traces during (12 msec; upper line) and after the voltage steps (10 msec; lower line). *C*, The steady state current (I) to voltage (V) relation was obtained as described for Figure 2*B*, from the same cell as displayed in *A*.

slices was characterized by large inward currents (about 1 nA) activated by depolarizing voltage jumps that inactivated within 5 msec (5 out of 46 cells). In addition, these cells showed delayed rectifying outward currents. In the current-clamp mode, action potentials could be elicited following current injection (not shown), indicating that they were most likely neurons.

The third type of cells in P6–8 slices consisted of 9 out of the 46 cells analyzed. In this group, no voltage-activated currents could be activated by de- or hyperpolarizing voltage steps.

Membrane currents of cells from P10 to P13

The entrance potential of cells from P10 to P13 after establishing the whole-cell mode averaged -51 mV (range, -31 to -68 mV; $N = 35$). Cells in slices obtained from P10–13 mice exhibited a current pattern different from those from younger animals. In the majority of cells, both de- and hyperpolarizing current pulses activated outward and inward currents, respectively (28 out of 41 cells from 20 animals; Fig. 4*A*). The current decayed, and peak and steady state currents were linearly related to the holding potential. These passive properties are reflected in the almost linear steady state current–voltage relation, determined with a voltage ramp of 1 sec duration (Fig. 4*C*). Application of 10 mM Ba^{2+} to the bath completely blocked the decaying component of the inward and outward currents, indicating that it is carried by K^+ (Fig. 5).

In the remaining group, eight cells (i.e., 20%) showed a current

pattern as described for the majority of cells from P6 to P8 (delayed-rectifying outward current). As observed in the slices obtained from younger animals, the outward current inactivated ($N = 4$) in some cells; in others, no apparent inactivation was observed ($N = 4$). In one of the cells with noninactivating currents, an A-type K^+ current could also be isolated using the pulse protocol described above (not shown). Seven percent ($N = 3$) of cells did not show any voltage- or time-dependent currents. Two cells (4%) expressed only slowly decaying inward currents in response to hyperpolarizing commands. In none of the cells from that age were inward currents observed with depolarizing voltage steps, and thus it was not possible to elicit action potentials.

Analysis of the current decay of cells from P10 to P13

We have further analyzed the properties of the currents that are characteristic for the majority of cells recorded from slices of P10–13 mice (Fig. 4*A*). The inward and outward currents, activated with hyperpolarizing or depolarizing voltage steps, decayed with time constants ranging from 10 to 40 msec. This variability of the time constant was apparent when comparing values obtained from different cells. In contrast, the time constants obtained from one cell were independent of the membrane potential (Fig. 4*B*). Moreover, when the membrane potential was switched back from the depolarized value to the holding potential, an inward current was elicited that decayed with a

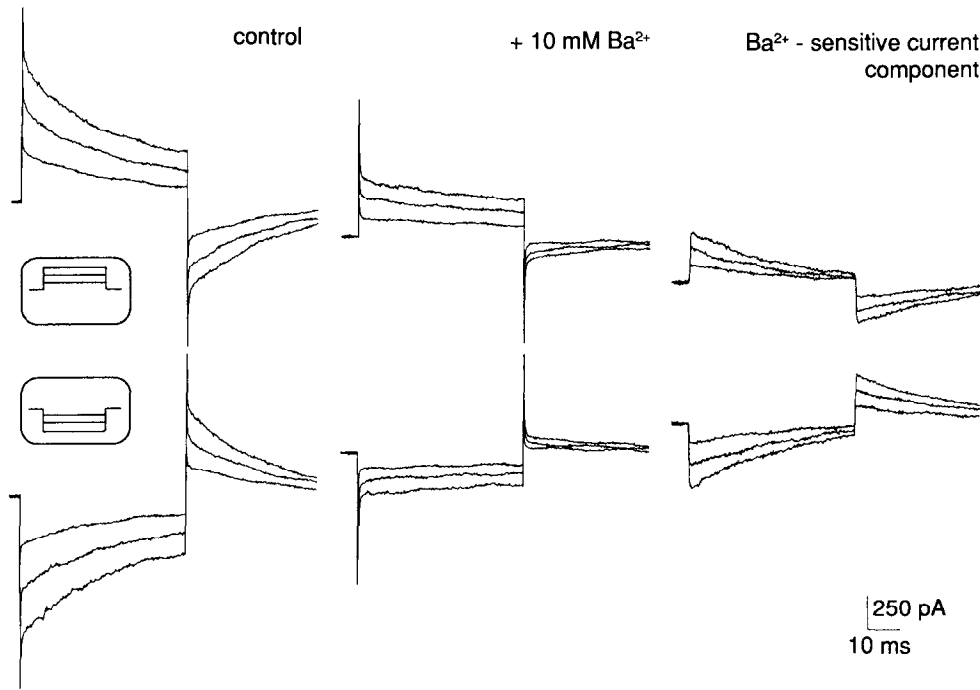


Figure 5. Effect of Ba^{2+} on currents from a cell of P11. Currents were activated and displayed as described for Figure 2, in standard bathing solution (control; left traces) and in the presence of 10 mM Ba^{2+} (middle traces). The Ba^{2+} -sensitive current component was obtained by subtracting the family of current traces in the presence of Ba^{2+} from those in standard solution (right traces).

time course similar to the outward current elicited with the depolarizing voltage step. Conversely, stepping back from hyperpolarized potentials (which activated decaying inward currents) elicited an outward current. In the following, we have analyzed these tail currents in more detail.

The decaying component of the inward tail currents after a depolarizing voltage step, and surprisingly, also of the outward tail currents after a hyperpolarizing voltage step, was almost completely blocked by adding Ba^{2+} to the bath, indicating that

the current was carried by K^+ (Fig. 5). The finding that a K^+ inward and a K^+ outward current can be activated at the same membrane potential suggests that the equilibrium potential is shifted during the preceding voltage step. To test this assumption, the current reversal potential was determined (with the above-described tail current analysis) after a depolarizing voltage step to 20 mV (Fig. 6A). As can be seen in Figure 6B, the reversal potential is closer to the assumed E_K , (based on $[K^+]$ of the extracellular solution and the pipette solution) if the pre-

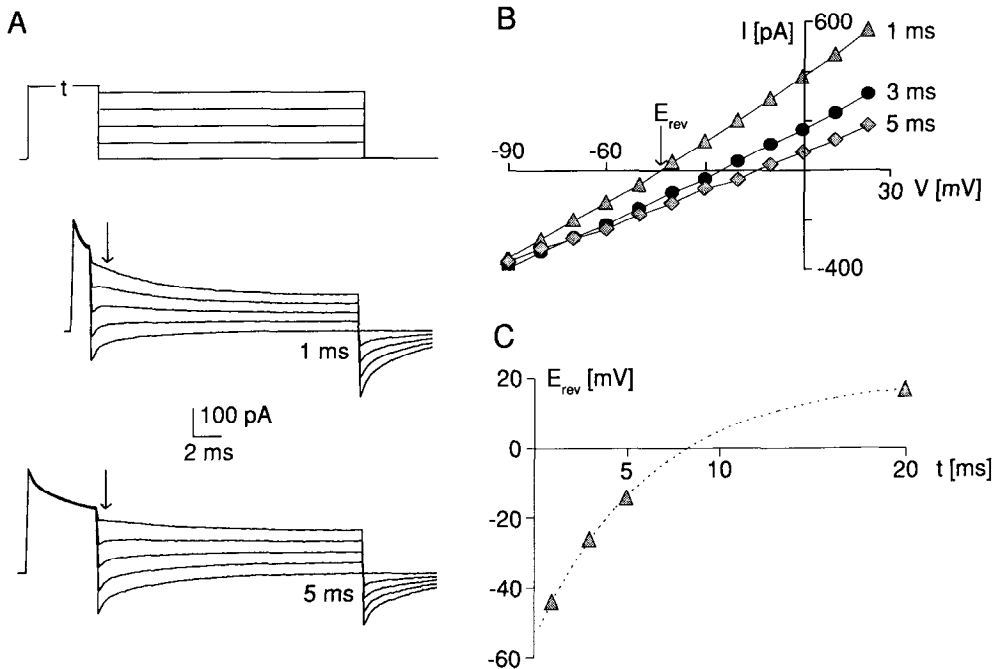
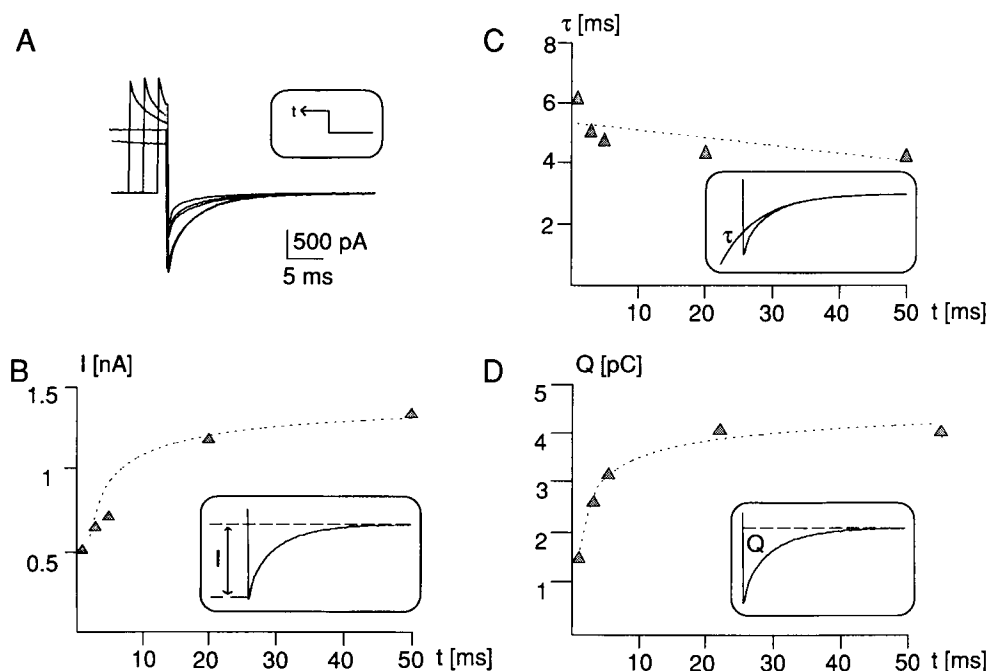


Figure 6. Dependence of the current reversal potential on the duration of a depolarizing pulse. *A*, The tail current protocol as described for Figure 3A was used to determine the reversal potential of outward currents. The membrane was clamped from a holding potential of -70 mV to 20 mV for 1 msec (middle traces) and 5 msec (lower traces). The pattern of voltage steps is indicated in the upper trace, and the time interval t was varied. *B*, From the recordings shown in *A*, the current amplitudes were determined briefly after the voltage step to 20 mV at the time indicated by the arrow in *A*. Currents (I) were plotted as a function of the membrane potential (V) for traces preclamped to 20 mV for 1 msec (triangles), 3 msec (circles), and 5 msec (squares). The current reversal potential (E_{rev}) for recordings preclamped for 1 msec is indicated. *C*, Current reversal potentials as determined in *B* were plotted as a function of the prepulse duration (indicated as t in *A*). The data points were fit by an exponential function. The theoretical reversal potential at $t = 0$ msec (no previous voltage jump) was at -56 mV.

Figure 7. Properties of the inward current activated after a depolarizing voltage jump. *A*, As described above, inward currents were activated after clamping from a depolarized potential (20 mV) to the holding potential (−70 mV). The dependence of the inward current on the duration of the depolarized voltage step was analyzed. Current recordings are superimposed that were first clamped for variable times t to 20 mV and, subsequently, to the holding potential. The step to the holding potential was synchronized to illustrate the difference in the superimposed traces of inward currents. *B*, From recordings as shown in *A*, the peaks of the inward current (I) were plotted as a function of the prepulse duration (t). The *inset* illustrates a sample record of the inward current after the prepulse. *C*, The time constants of the current decay measured 5–30 msec after the prepulse were plotted as a function of the prepulse duration (t). *D*, The integral of the decaying current between the offset of the prepulse and 30 msec thereafter, yielding the charge Q , was plotted as a function of the prepulse duration (t).



ceding voltage step is short (1 msec; Fig. 6*B*). With longer voltage steps, the reversal is shifted to more positive values. The plot of the duration of the prepulse versus the reversal potential indicates that a plateau is reached after about 20 msec. The extrapolated reversal potential at $t = 0$ msec is about −60 mV (Fig. 6*C*), indicating a $[K^+]_o$ of 14 mM according to the Nernst equation. Since the bath solution contained 5.4 mM K^+ , an additional decrease in intracellular $[K^+]$ during the voltage step cannot be excluded. We conclude that, because of current activation, the transmembrane K^+ gradient is shifted to more positive values with depolarizing voltage steps and to more negative values with hyperpolarizing voltage steps.

We varied the time of a prepulse to study the peak amplitude and the time constant of the decaying tail current after the clamp command back to the holding potential (Fig. 7*A*). The peak amplitude increased with increasing prepulse duration (Fig. 7*B*), while the time constant of decay was not affected (Fig. 7*C*). From the integral of the decaying tail current, the charge transferred across the membrane could be determined. This value increased with increasing time of the prepulse and reached a plateau after about 20 msec (Fig. 7*D*).

Morphological properties of cells from P6 to P8

Light microscopy

Cells with the outward rectifying current pattern (69% of the electrophysiologically studied cells) revealed characteristic morphological features when filled with LY. They had a round to oval-shaped perikaryon from which numerous thin processes extended. By focusing, these processes were seen to extend approximately radially from the cell body, with no preferred di-

rection. Many of their thin processes revealed numerous “swellings” reminiscent of (neuronal) varicosities. Figure 8 shows a typical cell with outward rectifying properties (Fig. 8*A*; cf. Fig. 2*A*). Figure 8*B* and *C*, shows the corresponding LY-filled cell; the micrographs were taken at different focal depths. The “swellings” of the processes are clearly visible.

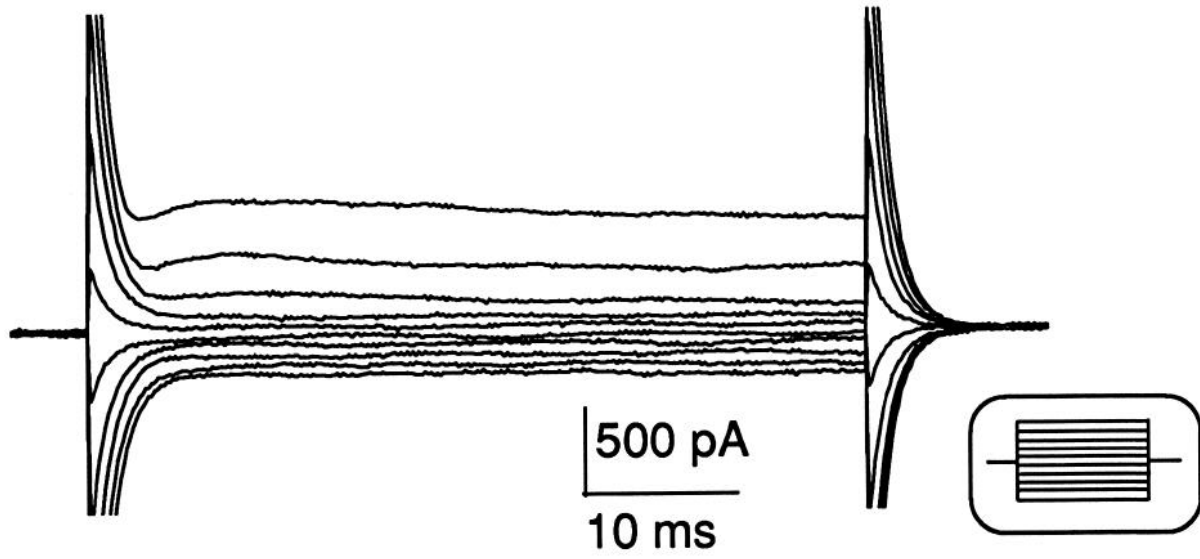
These “swellings” were again seen in 1 μm -thick Epon sections that were prepared after replacing LY fluorescence by an insoluble electron-dense product (Fig. 8*D,E*). In the micrographs shown in Figure 8, *D* and *E*, arrows point to labeled “swellings” and short processes. The labeled cell body is not visible, because it is not present in this section.

Handling of the slices during electrophysiology as well as during the photooxidation process required protocols that were not optimal for electron microscopy. Thus, the preservation of the tissue processed for electron microscopy was not always satisfactory. Five DAB-labeled P6 glial cells characterized electrophysiologically in slices could be evaluated ultrastructurally.

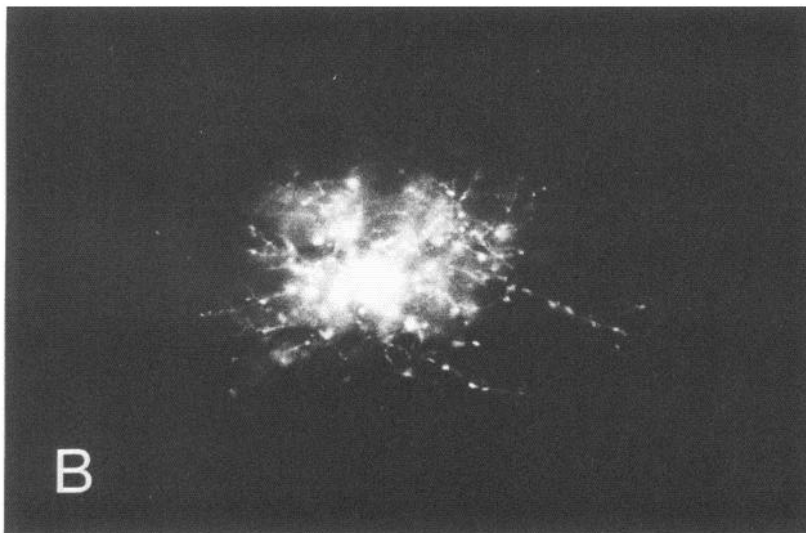
Ultrastructural observation at P6

The corpus callosum of P6 mice is composed of loosely arranged unmyelinated axons, characterized by the presence of few microtubules, and scattered glial cells. Although more than 100 glial cells were evaluated in this material, only one cell could unequivocally be identified as astrocyte, due to the presence of intermediate filaments in its perikaryon. All other cells could not be classified at this early stage of development, for the following reasons. They contained no detectable amounts of intermediate filaments or glycogen, which are features of more mature astrocytes. This is in accord with the observation that

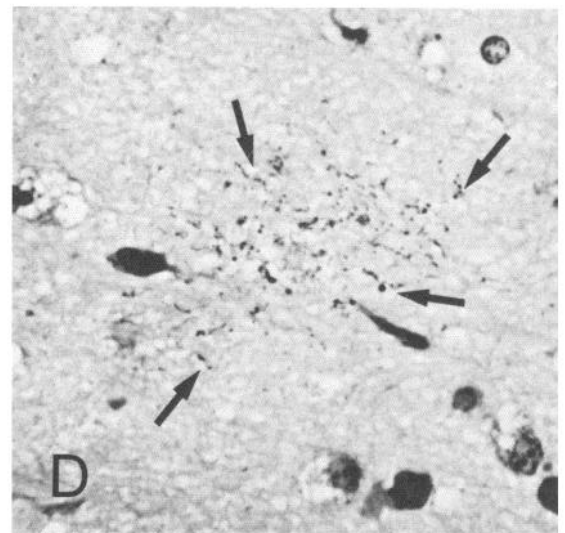
Figure 8. Electrophysiological and morphological properties of a cell from a P6 mouse corpus callosum. *A*, Voltage-activated potassium currents displayed as described for Figure 2*A*. *B* and *C*, LY-filled P6 glial cell. Both micrographs represent the same frame but were taken at different focal depths. Radially oriented processes extending from the perikaryon bear numerous “swellings.” *D* and *E*, One micron-thick Epon sections, Nissl stained: LY-filled P6 glial cell, photoconverted to an electron-dense diaminobenzidine (DAB) reaction product. The micrograph shown in *D* was



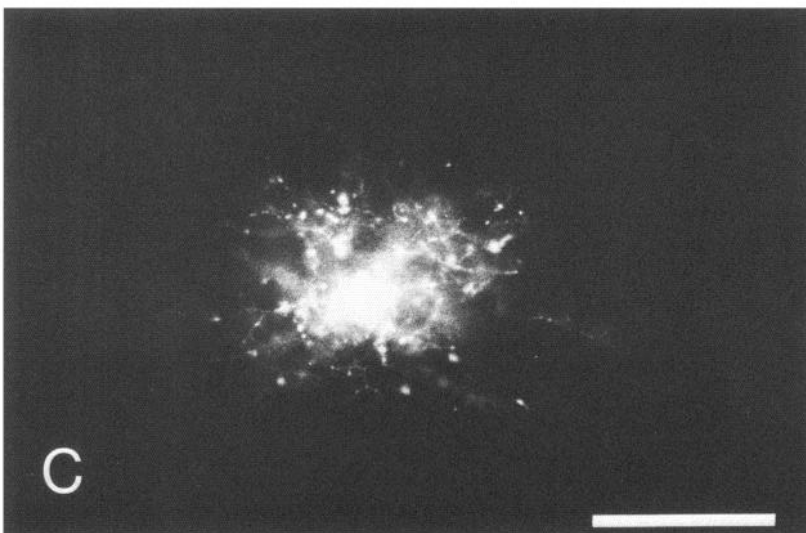
A



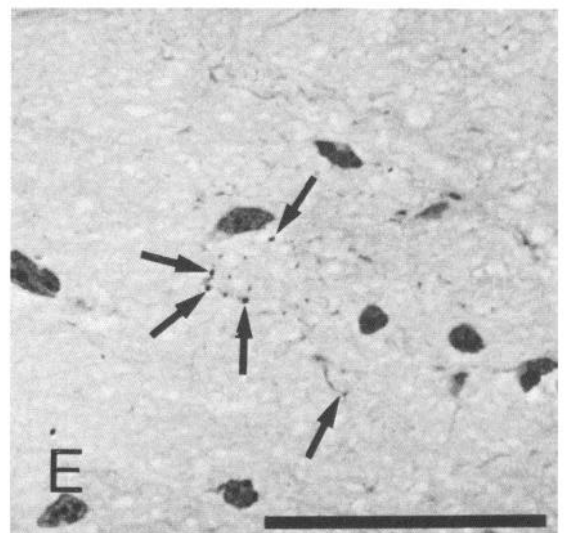
B



D



C



E

derived from a section close to the cell body; *E* was taken about 15 μm apart from the cell body. Arrows point to the DAB-labeled "swellings." Scale bars, 50 μm .

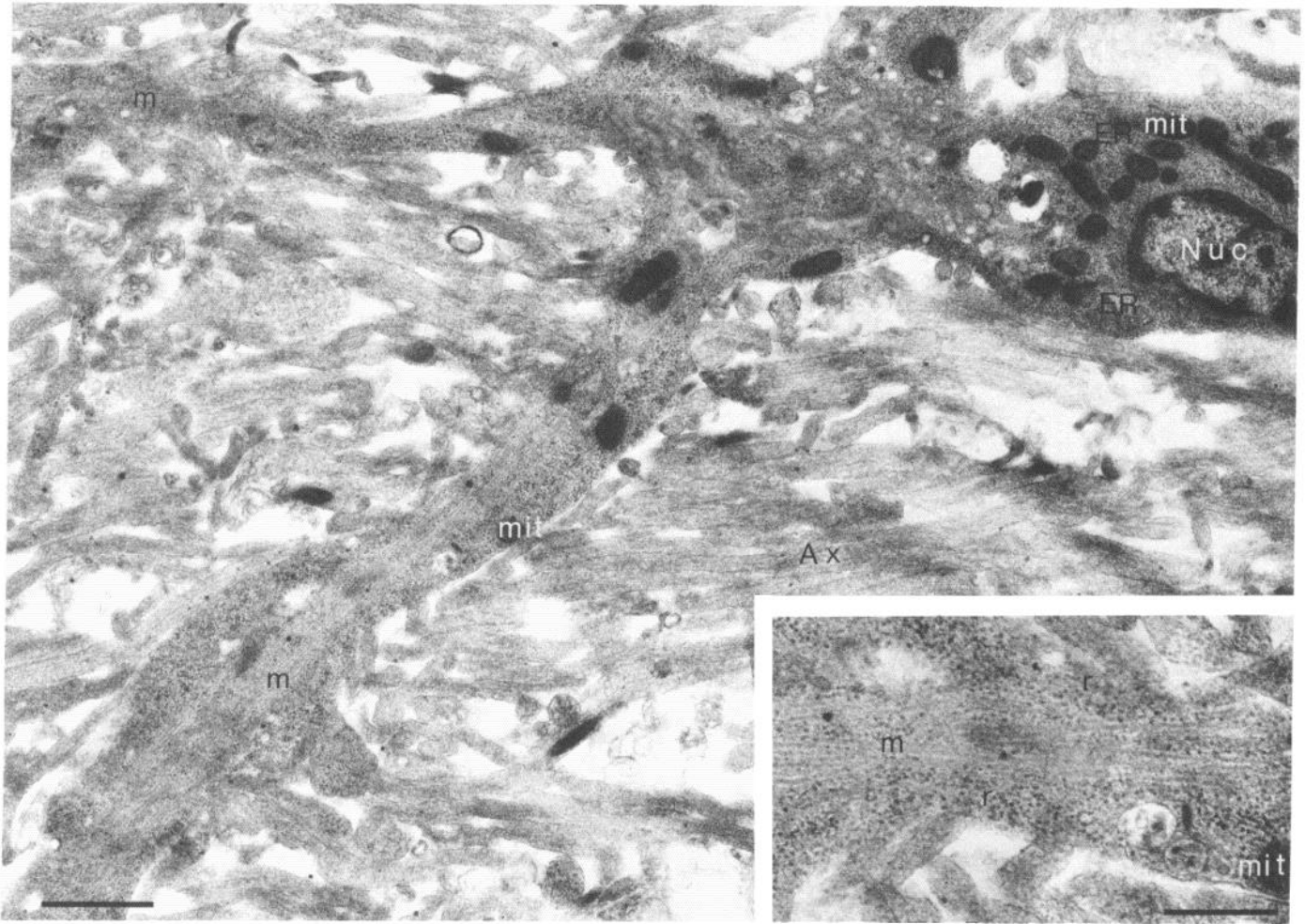


Figure 9. Electron micrograph showing an undifferentiated glial cell present in a P6 corpus callosum. The perikaryon is rich in mitochondria (*mit*), rough endoplasmic reticulum (*ER*), and free ribosomes (*r*). The broad processes extending from the cell body are loaded with microtubules (*m*) and free ribosomes. Scale bar, 1 μm . The *inset* shows one of these processes at higher magnification. Scale bar, 0.5 μm . *Nuc*, nucleus; *Ax*, unmyelinated axons.

antibodies to glial fibrillary acidic protein stained only few cells in the corpus callosum of P6 mice using indirect immunofluorescence (J. Schnitzer, unpublished observation). The vast majority of somata in the corpus callosum resembled undifferentiated glial cells or glioblasts (see Sturrock, 1976; but see also Peters and Vaughn, 1967; Vaughn and Peters, 1967; Skoff et al., 1976). Their cytoplasm was rich in rough endoplasmic reticulum (*ER*), mitochondria, and free ribosomes. Some cells had broad processes emanating from the perikaryon, with numerous microtubules and free ribosomes, and some scattered mitochondria. Figure 9 shows a typical cell from a P6 corpus callosum. One should keep in mind that, although the abundance of microtubules is characteristic for mature oligodendrocytes, immature astrocytes have the same feature (Peters et al., 1976). The cytoplasm of some glial cells was darker than that of others, but no perikaryon could be defined unequivocally as being that of an oligodendrocyte.

Electron microscopy of DAB-labeled cells from P6 to P8

The reaction product in the DAB-labeled cells was so dense that cellular organelles were difficult to resolve. It was, however, easy to follow the course of their labeled cellular processes. Some of

them were aligned parallel to the axons building the corpus callosum (Fig. 10*A*); other processes from the same cell extended orthogonally to axons. The apparent "swellings" of the processes that were seen in the light microscope turned out to be due to mitochondria, some of which were considerably larger than the remainder of the labeled processes (Fig. 10*B*). The presence of large mitochondria in otherwise rather thin cellular processes was a characteristic feature of DAB-labeled cells. In some cases, DAB-labeled processes were found that "enwrapped" several axons (Fig. 10*C*). In the same material, we found few *unlabeled* glial processes (characterized by the abundance of free ribosomes) that "enwrapped" axons (Fig. 10*D*).

Morphological properties of cells from P10 to P13

Light microscopy

We investigated the morphological profile of cells from P10 to P13 that exhibited the predominant current pattern, the decaying inward and outward currents as described above (see also Figs. 11*A*, 12*A*). The morphology of the LY-filled cells from that age was different to that seen in P6–8 cells. The processes were not radially oriented, but were oriented predominantly in a single direction, and most processes of a single cell extended

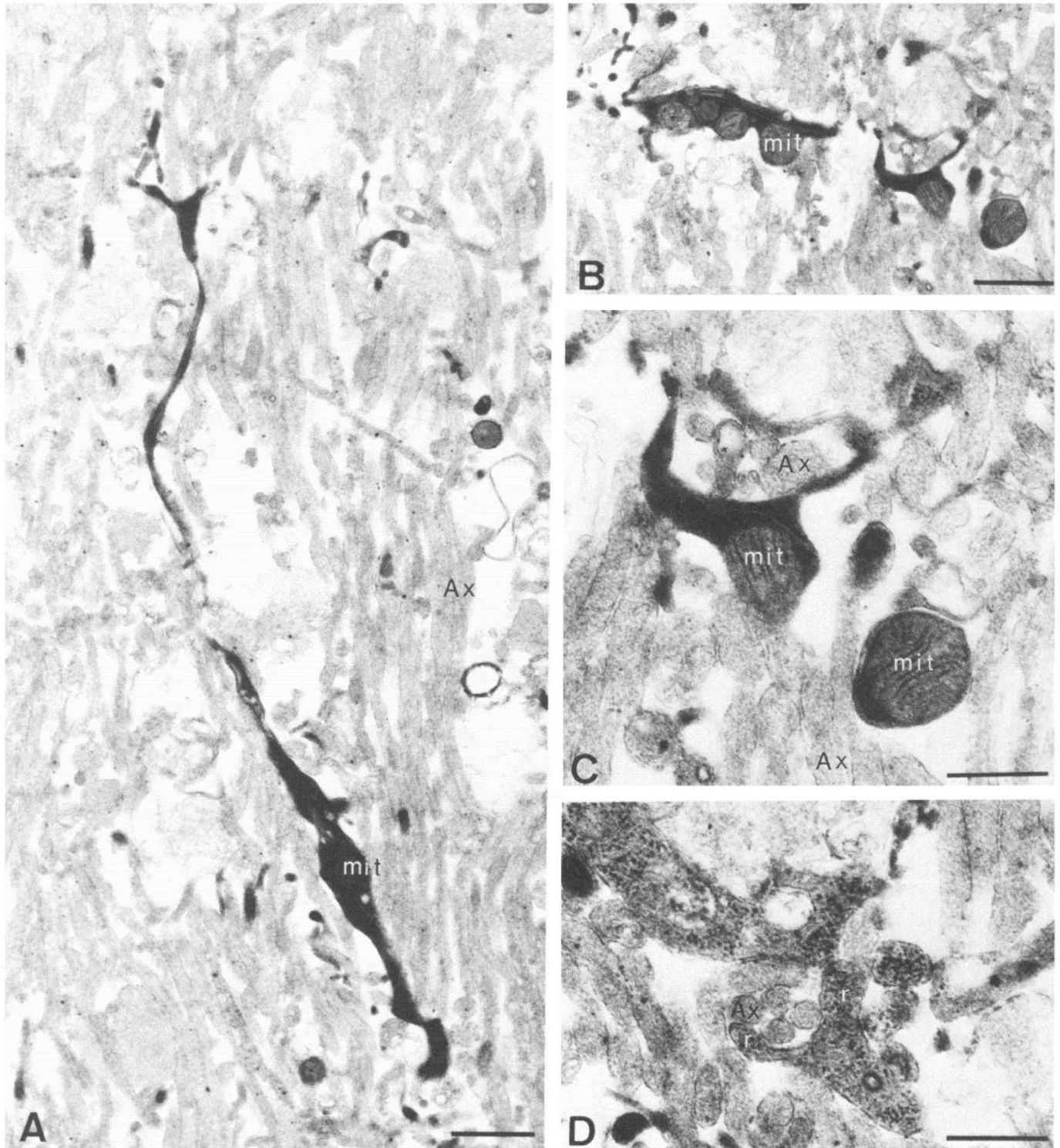


Figure 10. Electron micrographs from a P6 corpus callosum: LY-filled processes from a P6 glial cell, photoconverted (*A–C*), and unlabeled processes (*D*). *A*, A photoconverted DAB-labeled process follows the course of the unmyelinated axons (*Ax*) that run from *top* to *bottom* in this micrograph. *B*, Some parts of the photoconverted DAB-labeled P6 glial cell processes contain numerous large mitochondria (*mit*). *C*, A photoconverted P6 glial cell process “enwrapping” axons. *D*, An unlabeled glial cell process characterized by the presence of numerous free ribosomes (*r*; cf. Fig. 9, inset) surrounds unmyelinated axons. Scale bar: *A* and *B*, 1 μm ; *C* and *D*, 0.5 μm .

parallel to each other (Figs. 1*C*; 11*B,C*; 12*B*). After photoconversion, it was possible to see in semithin sections that the nucleus of these cells had an excentric location in the perikaryon; their DAB-labeled processes were easy to identify (Fig. 12*C*).

Ultrastructural observation at P10

Preservation of the tissue was again not always satisfactory, but the glial cell perikarya seen at P10 in the electron microscope

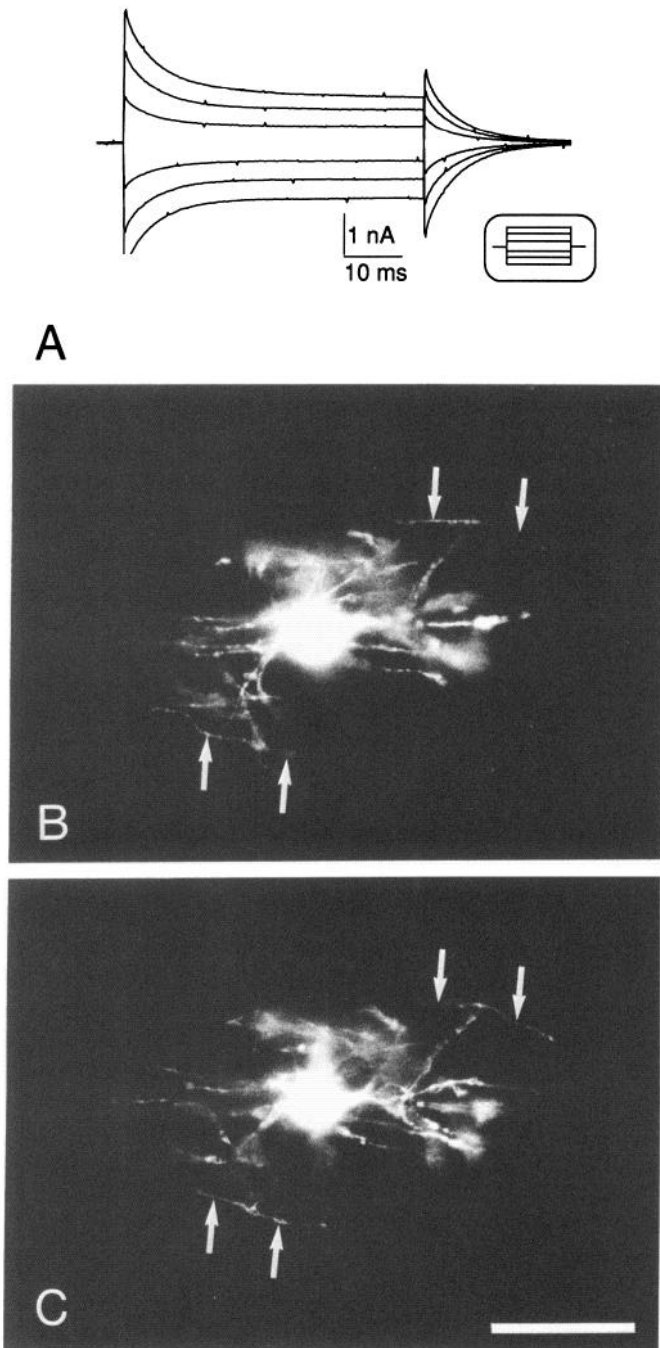


Figure 11. Electrophysiological and morphological properties of a P10 glial cell present in the corpus callosum. *A*, Voltage-activated potassium currents displayed as described for Figure 2*A*. *B* and *C*, LY-filled P10 glial cell. Most of its processes extend parallel to each other. Both micrographs represent the same frame but were taken at different focal depths. Arrows point to parallel processes. Scale bar, 50 μm .

were usually preserved well enough to allow the classification of some of them. At this stage, astrocytes that had plenty of intermediate filaments and short, wide-bore cisternae of rough ER (Fig. 13; see also inset) were more frequently seen compared to P6. Other cells had well-developed Golgi cisternae, numerous mitochondria, and stacks of narrow-bore cisternae of rough ER, which might represent the first few oligodendrocytes seen at that

stage (not shown). Many perikarya could still not be classified unequivocally at this stage.

At P10, the vast majority of the callosal axons were unmyelinated. Many processes defined to be of glial origin because of their cellular components (free ribosomes, mitochondria, microtubules or intermediate filaments, and rough ER) were seen to be intermingled with callosal axons (Fig. 14). Similar to glial cell processes of P6 mice, at P10 some glial processes had large mitochondria (Fig. 14*C,D*). In a few cases the presence of filaments suggested an astrocytic nature (Fig. 14*D*). However, in most instances ribosomes and few microtubules were the only cellular organelles present in addition to mitochondria. The presence of these components was not sufficient to determine the nature of the glial cell processes (Fig. 14*C*).

Very few myelinated axons were present in the corpus callosum at P10 (Fig. 15; arrows point to DAB-labeled processes). All myelinated axons were considerably larger compared to unmyelinated axons in their neighborhood.

Electron microscopy of DAB-labeled cells at P10

In contrast to most unlabeled glial cell perikarya present in the corpus callosum material, the cytoplasm of the DAB-labeled cells was usually not well preserved. The only cellular organelles that could be identified were mitochondria (Fig. 16, upper third of the micrograph). Labeled processes were seen to “surround” axons. These axons tended to have a larger diameter than the majority of the unmyelinated callosal axons present at that stage (Figs. 13, 16, dark reaction product in apposition to larger axons). None of the electrophysiologically characterized, LY-labeled cells examined had established a myelin sheath.

Discussion

Comparison of currents from glial cells in vitro and in situ

This study provides the first tight-seal patch-clamp recordings from glial cells *in situ*. Using the loose-patch technique, Marrero et al. (1989) have recorded Na^+ and K^+ currents from the surface of the frog optic nerve. The origin of these currents was most likely from surface astrocytes. In our study, we have shown that the majority of glial cells of the corpus callosum obtained at a single developmental stage, that is, P6–8, have similar electrophysiological properties. These were different from the properties of most cells recorded in P10–13 slices. The morphological data that will be discussed below suggest that cells from P6 to P8 are glioblasts and cells from P10 to P13 are promyelinating oligodendrocytes. A comparison of our study with recordings of cortical oligodendrocytes and their precursors studied in cell culture (Sontheimer et al., 1989) shows similarities in the current-pattern expression during development. Glial precursor cells in culture identified with the stage-specific antibodies A2B5 and O4 express delayed-rectifying K^+ currents. Moreover, these cells are characterized by a strong outward rectification of the membrane currents. Such a current pattern was found in the majority of cells of the P6–8 corpus callosum.

In culture, two stages of precursor cells were distinguished: immature precursors, characterized by the expression of A2B5 antigen and the lack of expression of O4 antigen, showed in addition to the delayed-rectifying K^+ currents also Na^+ currents and in minor cases A-type K^+ currents. The later stage, the O4-positive precursors, expressed Na^+ currents in 26% and A-type K^+ currents in 45% of the cells tested (Sontheimer et al., 1989). Cells from the corpus callosum of P6–8 mice did not exhibit A-type K^+ currents and rarely Na^+ currents. They can thus be

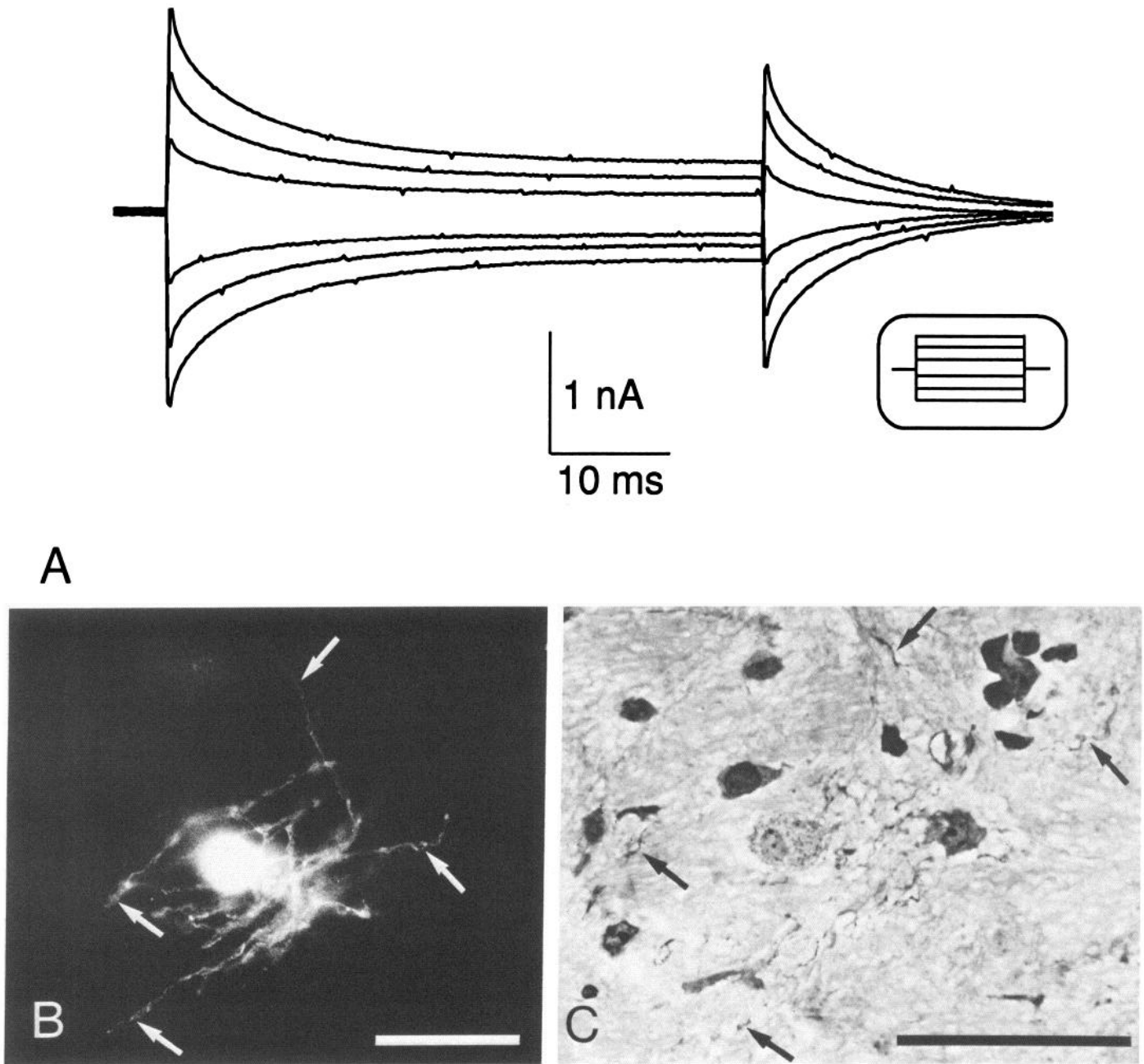


Figure 12. Electrophysiological and morphological properties of a P10 glial cell present in the corpus callosum. *A*, Voltage-activated potassium currents displayed as described for Figure 2*A*. *B*, LY-filled P10 glial cell. *Arrows* point to processes seen in *C*. *C*, This micrograph shows parts of the LY-filled cell and its processes after photoconversion in a $1\ \mu\text{m}$ -thick Epon section. Scale bars, $50\ \mu\text{m}$.

best compared to late precursor cells in cell culture. In this study, cells with Na^+ currents have not been extensively characterized on electrophysiological and morphological bases. They are probably more abundant in earlier developmental stages, which we intend to study in the future.

With the expression of the O1 antigen and the commitment of the cell to the oligodendrocytic lineage, the cultured cells markedly change their channel pattern: they express an only slightly voltage-dependent K^+ channel (Sontheimer and Kettenmann, 1988; Sontheimer et al., 1989). A similar current pattern is found in the majority of cells from P10–13 corpus callosum slices. The whole-cell currents measured in this study are in perfect agreement with the properties of single K^+ channels re-

corded from oligodendrocytes of mouse spinal cord explant cultures (Kettenmann et al., 1984). Only few cells of P10–13 slices show a current pattern reminiscent of that seen in P6–8 slices. The cause of the current decay during de- and hyperpolarizing voltage jumps that is seen in most P10–13 glial cells in the slice is not as pronounced in culture and will be discussed below. Thus, the pattern of channel development is similar in cultured cells and in the intact corpus callosum.

Morphological properties of the electrophysiologically studied cells

We have shown that LY-filled glial cells from P6–8 slices were morphologically different from those cells from P10–13 mice.

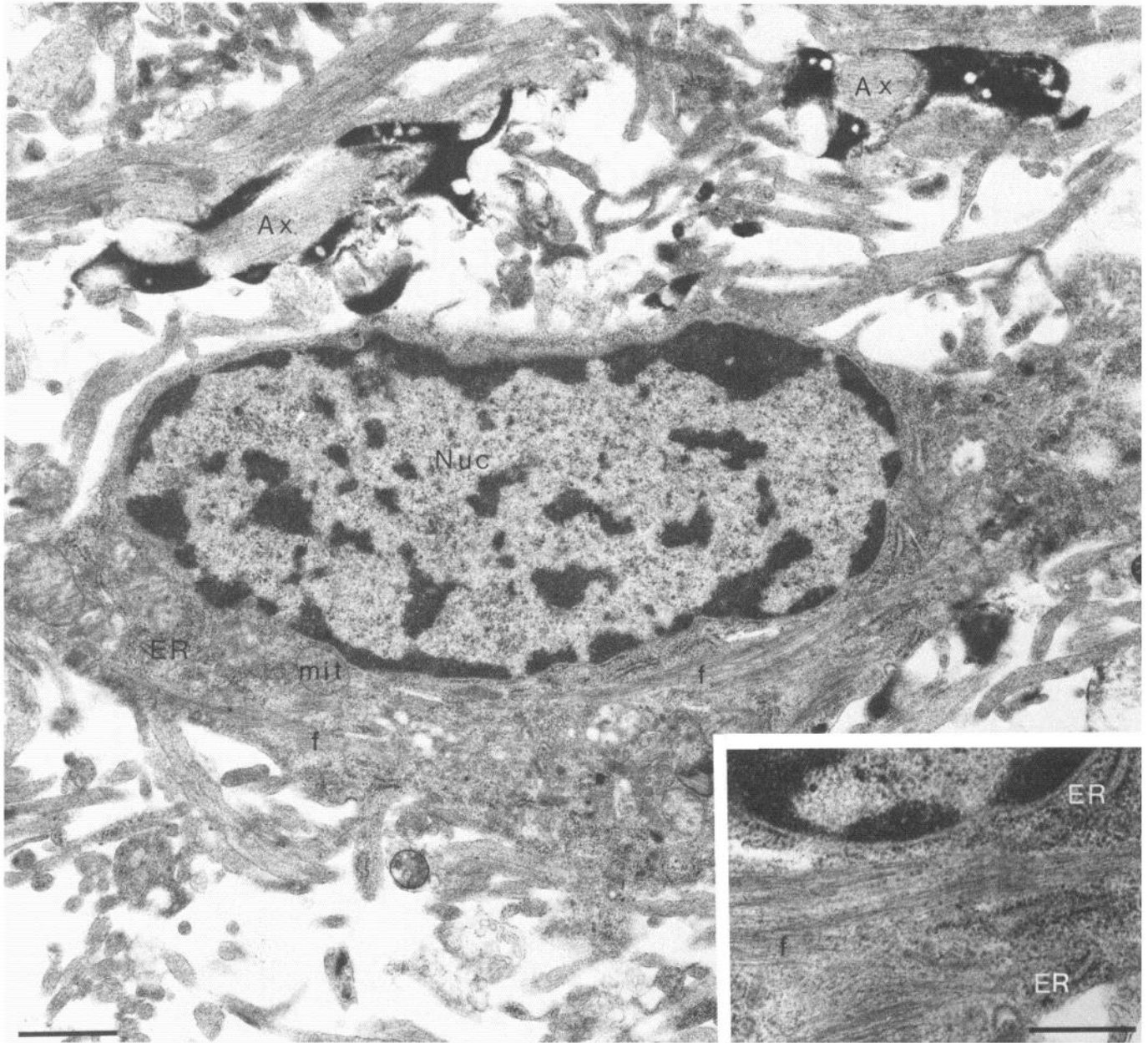


Figure 13. Electron micrograph of the corpus callosum of a P10 mouse brain. Cells with features characteristic of astrocytes [i.e., numerous intermediate filaments (*f*), short wide-bore cisternae of rough endoplasmic reticulum (*ER*), free ribosomes, and few mitochondria (*mit*); see also *inset* at higher magnification] are readily seen. The *dark labeling* (top of the micrograph) that “surrounds” axons (*Ax*), characterized by the presence of microtubules, represents LY-filled photoconverted P10 glial cell processes. Note that the axons surrounded by these processes are considerably larger compared to most of the unmyelinated axons in the corpus callosum seen at this stage. *Nuc*, nucleus. Scale bars: 1 μm ; *inset*, 0.5 μm .

At P6, they had numerous thin processes extending approximately radially from their soma, while most processes of cells at P10–13 extended parallel to one another. We will discuss below why we suggest that most of the electrophysiologically characterized cells from P6–8 slices are by morphological criteria glioblasts, while most of the cells from P10 to P13 are by morphological criteria promyelinating oligodendrocytes.

Handling of the tissue during electrophysiology and photooxidation was not ideal for the preservation of the ultrastructure, but most unlabeled glial somata were preserved well enough to examine their cytological properties. This is in contrast to many LY-labeled photoconverted cells. Their cytoplasm was

often disrupted to such an extent that it was impossible to discover characteristic cytoplasmic features. In addition, the photooxidation product was so dense that it masked cytological details.

In the corpus callosum of P6 mice, the majority of the somata represent immature glial cells (Sturrock, 1976). We found that at this stage most glial cells contained organelles that are characteristic of immature glia, that is, numerous mitochondria, single cisternae of rough ER, and free ribosomes (Skoff et al., 1976; Sturrock, 1976; Skoff, 1990). Microtubules that are characteristic for oligodendrocytes (Peters et al., 1976) but also for glioblasts (Peters and Vaughn, 1967; Vaughn and Peters, 1967;

Skoff et al., 1976; Sturrock, 1976; Skoff, 1990) were frequently seen. Thus, by P6 most glial cells lacked features characteristic of mature astrocytes (i.e., filaments or glycogen granules) or mature oligodendrocytes (i.e., dark cytoplasm, stacks of rough ER) (see Peters et al., 1976). At P5, only about 5% of all perikarya were defined as being young astrocytes (Sturrock, 1976), which is in accord with our observation that very few cells with glial filaments were seen at P6. Thus, cells at P6 could either comprise young astrocytes, which are rare, or more likely glioblasts, which make up more than 95% of all cells at that stage.

At P6, LY-labeled and unlabeled glial cell processes were seen that "enwrapped" several unmyelinated axons. Numerous free ribosomes but no further organelles were seen in those "enwrapping" processes. It was thus not possible to decide unequivocally whether they belonged to astrocytes that lacked filaments in their finest processes or to immature glial cells. However, since astrocytes have only few free ribosomes compared to immature glial cells (Sturrock, 1976), we suggest that the cellular processes that "enwrap" axon bundles more likely belong to immature glia than to young astrocytes. In conclusion, we suggest that the glial cells from P6–8 slices that possess electrophysiological properties of cultured O4-positive precursor cells are by morphological criteria glioblasts. Interestingly, polyribosomes were observed in oligodendrocytic processes, in the proximity of the forming myelin sheaths (Waxman and Sims, 1984). Since oligodendrocytes are not present at P6, we can only speculate as to whether the glioblasts "enwrapping" axon bundles at this stage are already determined to differentiate into oligodendrocytes. We have no evidence of whether these glioblasts are bipotential progenitor cells (Raff et al., 1983) like the O4-positive precursor cells *in vitro* (Trotter and Schachner, 1989). Electrophysiological studies on developing type 1 astrocytes (Raff et al., 1983) have to be performed *in situ* to understand whether astroblasts are similar to or different from glioblasts differentiating into oligodendrocytes.

Another feature of LY-filled glioblasts was the presence of numerous "swellings" of their thin processes, which turned out to be large mitochondria. We cannot exclude the possibility that these mitochondria are artificially swollen due to the handling of the slices, since immature corpus callosum tissue is very fragile and sensitive to fixation conditions (Berbel and Innocenti, 1988). We have also seen them, however, in unlabeled glial cell processes, which suggests that it is neither the LY-filling nor the electrophysiological recording that might cause a swelling.

At P10, undifferentiated glial cells were still the dominant cell type found in the corpus callosum; astrocytes and oligodendrocytes were rare, and few axons had acquired a myelin sheath. This is in accordance with Sturrock (1976). Many glial cells showed electrophysiological properties reminiscent of oligodendrocytes *in vitro* (Sontheimer et al., 1989). A first hint that these cells might be oligodendrocytes was the excentric location of their nucleus, which is a characteristic feature of oligodendrocytes (Peters et al., 1976; Skoff et al., 1976). Electron microscopic observations showed that their processes surrounded single axons. These axons were considerably thicker compared to the mean diameter of the unmyelinated axons in their neighborhood and were thus in the range of the mean diameter of the first few myelinated axons present at that stage. In the corpus callosum of mice, where even by the end of the eighth postnatal month only 28% of the axons are myelinated, it was described that the myelinated axons always have a larger mean axon diameter

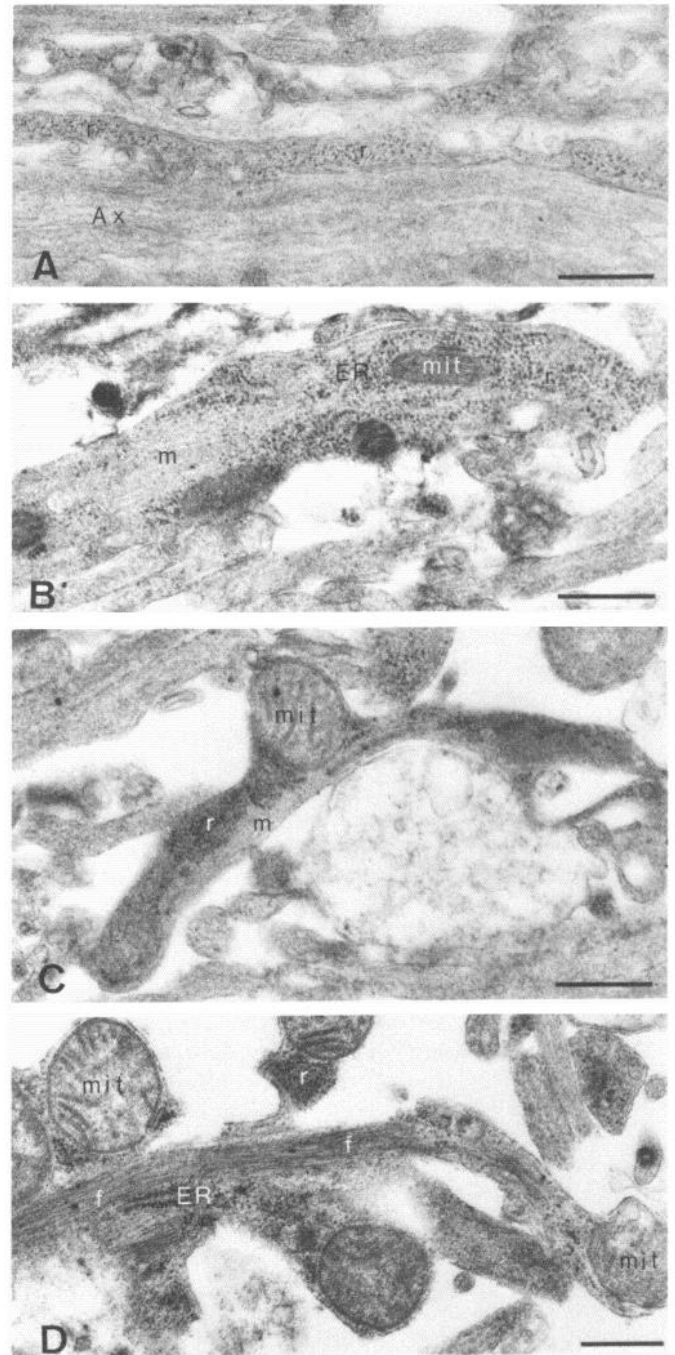


Figure 14. Electron micrographs of glial cell processes in the corpus callosum of a P10 mouse brain. *A*, Glial cell processes with numerous free ribosomes (*r*) running parallel to callosal axons (*Ax*). *B*, Broad glial cell process with numerous microtubules (*m*), mitochondria (*mit*), rough ER, and free ribosomes. *C*, Nonclassified glial cell process with few microtubules, ribosomes, and a large mitochondrion. *D*, An astroglial process with filaments (*f*), rough ER, and large mitochondria. Scale bars, 0.5 μ m.

compared to unmyelinated axons (Sturrock, 1980). In the optic nerve, it is known that axons increase in size prior to myelination (Arees, 1978). It is therefore likely that the processes of the LY-filled, photoconverted cells from P10 slices that surround rather thick axons represent the first loop of an oligodendrocytic process surrounding a promyelinated axon (Sturrock, 1975). We

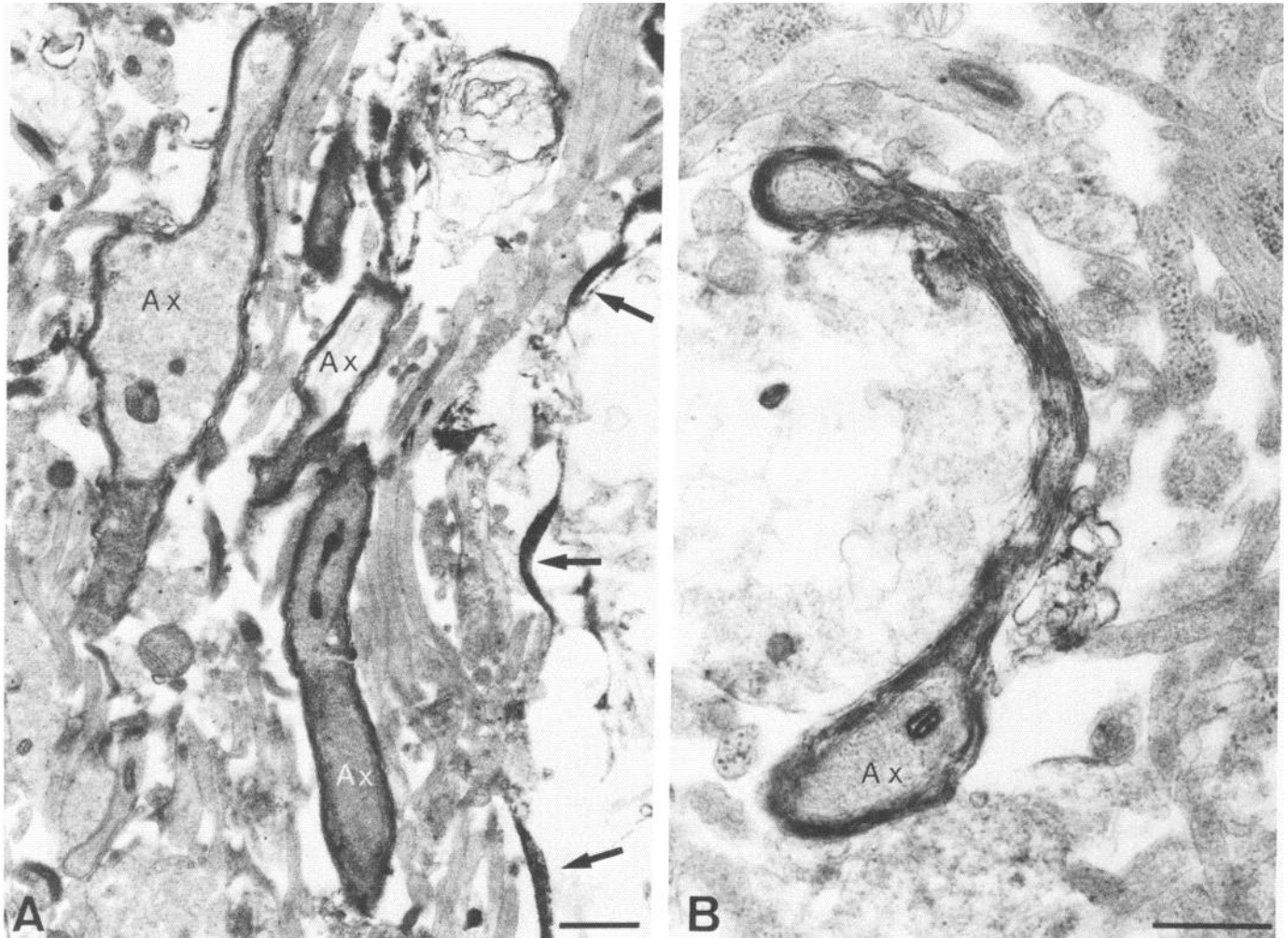


Figure 15. Electron micrographs of the corpus callosum of a P10 mouse brain. In *A*, arrows point to a LY-filled, converted P10 glial cell process that is in the proximity of three myelinated axons (*Ax*). *A* and *B*, The diameters of myelinated axons are usually larger than those of unmyelinated axons. Scale bars: *A*, 1 μm ; *B*, 0.5 μm .

suggest that the glial cells from P10–13 slices that possess electrophysiological properties of O1-positive oligodendrocytes in culture are by morphological criteria promyelinating oligodendrocytes.

By injecting LY and HRP into glial cells of the adult rat optic nerve, Ransom and co-workers demonstrated the three-dimensional and ultrastructural features of oligodendrocytes *in situ* (Butt and Ransom, 1989; Ransom et al., 1991). These oligodendrocytes had longitudinally oriented processes that were 150–200 μm long. In our study, promyelinating oligodendrocytes had longitudinally oriented processes as well, but their length was shorter, being about 50–70 μm long (Figs. 1; 11*B,C*, arrows). This suggests that the processes of oligodendrocytes as they establish their first loop around axons have not reached their final length, and that they will become longer with further maturation.

None of the LY-labeled photoconverted glial processes were in contact with myelinated axons. This is not unexpected since less than 0.2% of the callosal axons are myelinated around P10 (Sturrock, 1980). The chance to “select” for electrophysiological studies one of the few oligodendrocytes that have already established a number of myelin lamellae is probably low.

The observation that by P10 some glial cells revealed elec-

trophysiological properties of cultured glial precursors is in accord with the fact that at P11 about 70% of the glial somata in the corpus callosum are undifferentiated glial cells (Sturrock, 1976). Even at adulthood, some immature glial cells that are capable of division are present in the corpus callosum of mice (McCarthy and Leblond, 1988).

The presence of neurons in the early corpus callosum

Neurons and neuroblasts are migrating through the corpus callosum on their way from the subependymal zone to their target in the cortex (Altman, 1966). Thus, based on morphological studies, 15% of cells in the newborn mouse are neurons, decreasing to less than 1% 5 d after birth (Sturrock, 1976). In our electrophysiological study, 11% of cells from P6 to P8 were able to generate action potentials, thus identifying them as neurons, while no such cell was detected 10 d after birth. These cells were not characterized on their ultrastructural basis.

K⁺ movements are the reason for current decay during a voltage jump in P10–13 mice

In oligodendrocytes of slices of P10–13 corpus callosum, outward and inward currents corresponding to de- and hyperpolarizing voltage jumps showed a marked decay. Such a behavior

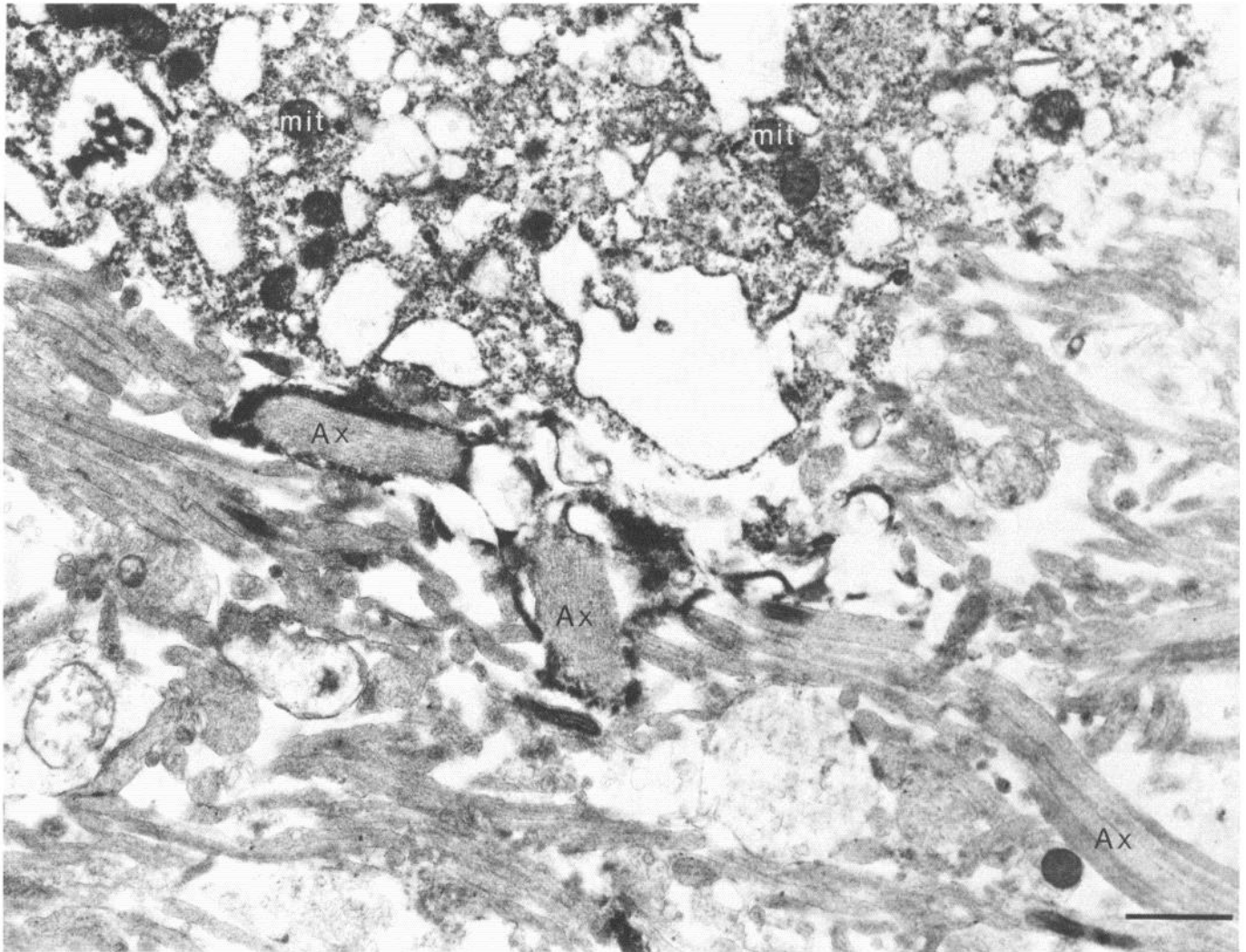


Figure 16. Electron micrograph of a LY-filled, photoconverted P10 glial cell in the corpus callosum. The corresponding LY-filled cell is shown in Figure 12, *B* and *C*. The upper third of the micrograph shows part of the dark, "granulated" oligodendrocyte cytoplasm, which is rather disrupted. Numerous mitochondria (*mit*) are the only cellular organelles that can be identified clearly. Close to the perikaryon, labeled processes "surround" callosal axons (*Ax*), which are considerably larger compared to most axons seen at that stage. Scale bar, 1 μm .

was not observed in oligodendrocytes from cultures of mouse cortex (Sontheimer et al., 1989). A slight decay was observed in oligodendrocytes of 4–6 week-old spinal cord cultures (Sontheimer and Kettenmann, 1988). We infer from several observations that the current decay is due not to inactivation, but to a shift of the K^+ gradient across the membrane.

(1) After a voltage jump, the reversal potential has shifted. It is more positive with depolarizing voltage jumps and more negative with hyperpolarizing voltage jumps. This is compatible with an outward movement of K^+ during depolarization and an inward movement during hyperpolarization.

(2) The time constant of decay is independent of voltage, but varies markedly from cell to cell. Moreover, the time constant of current decay after the voltage jump shows a similar behavior. Since the cell is dialyzed by the pipette solution, and since the extracellular space is smaller than the intracellular compartment, it seemed more likely that changes in $[\text{K}^+]_o$ occur extracellularly. Our results cannot exclude, however, that the change in the transmembrane potassium gradient could also partially be caused by a decrease in $[\text{K}^+]_i$.

The capacity of these promyelinating oligodendrocytes to move large amounts of K^+ across the membrane indicates that these cells can efficiently buffer $[\text{K}^+]_o$ by spatial buffer currents. These cells can thus serve as efficient regulators of $[\text{K}^+]_o$, as previously inferred from data on cultured glial cells. Cells from P6 to P8 did not show a shift in the transmembrane K^+ gradient. The reason could be that in immature tissue $[\text{K}^+]_o$ is not building up in the extracellular space, suggesting that this space is not yet as condensed as after P10. This is in line with the observation that in culture, where the extracellular space is almost infinite, such decaying currents were not or only marginally observed.

Advantages of the corpus callosum slice for the study of glial cell function

In this study, we have used the corpus callosum slice preparation to study membrane properties of oligodendrocytes *in situ* with patch-clamp recording techniques. This structure, in addition to the optic nerve, offers the unique advantage of easily recognizable glial cells, since in the corpus callosum after P5 99% of the cell bodies are glial. Moreover, this preparation can be easily

used to study membrane properties during the development of oligodendrocytes. Since the formation of myelin in the mouse corpus callosum occurs late after birth, a comparison of slices obtained from animals of different postnatal ages will yield a comparison of oligodendrocytes at different developmental stages. This preparation can also be used to study a signal transfer between neurons and glial cells with electrophysiological methods, since neuronal fiber tracts can be easily stimulated.

References

- Altman J (1966) Proliferation and migration of undifferentiated precursor cells in the rat during postnatal gliogenesis. *Exp Neurol* 16:263–278.
- Areas EA (1978) Growth patterns of axons in the optic nerve of chick during myelinogenesis. *J Comp Neurol* 180:73–84.
- Barres BA, Chun LLY, Corey DP (1990) Ion channels in vertebrate glia. *Annu Rev Neurosci* 13:441–474.
- Berbel P, Innocenti GM (1988) The development of the corpus callosum in cats: a light- and electron-microscopic study. *J Comp Neurol* 276:132–156.
- Butt AM, Ransom BR (1989) Visualization of oligodendrocytes and astrocytes in the intact rat optic nerve by intracellular injection of Lucifer yellow and horseradish peroxidase. *Glia* 3:470–475.
- Chiu SY, Wilson GF (1989) The role of potassium channels in Schwann cell proliferation in Wallerian degeneration of explant rabbit sciatic nerves. *J Physiol (Lond)* 408:199–222.
- Connor JA, Stevens CF (1971) Voltage clamp studies of a transient outward membrane current in gastropod neural somata. *J Physiol (Lond)* 213:21–30.
- Edwards FA, Konnerth A, Sakmann B, Takahashi T (1989) A thin slice preparation for patch clamp recordings from neurones of the mammalian central nervous system. *Pfluegers Arch* 414:600–612.
- Hamill OP, Marty A, Neher E, Sakmann B, Sigworth FJ (1981) Improved patch-clamp techniques for high-resolution current recording from cells and cell-free membrane patches. *Pfluegers Arch* 391:85–100.
- Hille B (1984) Ionic channels of excitable membranes. Sunderland, MA: Sinauer.
- Kettenmann H, Orkand RK, Lux HD (1984) Some properties of single potassium channels in cultured oligodendrocytes. *Pfluegers Arch* 400:215–221.
- Maranto AR (1982) Neuronal mapping: a photooxidation reaction makes Lucifer yellow useful for electron microscopy. *Science* 217:953–955.
- Marrero H, Astion ML, Coles JA, Orkand RK (1989) Facilitation of voltage-gated ion channels in frog neuroglia by nerve impulses. *Nature* 339:378–380.
- McCarthy GF, Leblond CP (1988) Radioautographic evidence for slow astrocyte turnover and modest oligodendrocyte production in the corpus callosum of adult mice infused with ³H-thymidine. *J Comp Neurol* 271:589–603.
- Newman EA (1986) High potassium conductance in astrocyte endfeet. *Nature* 233:453–454.
- Orkand RK, Nicholls JG, Kuffler SW (1966) Effect of nerve impulses on the membrane potential of glial cells in the central nervous system of amphibia. *J Neurophysiol* 29:788–806.
- Peters A, Vaughn JE (1967) Microtubules and filaments in the axons and astrocytes of early postnatal rat optic nerve. *J Cell Biol* 32:113–119.
- Peters A, Palay SL, Webster HF (1976) The fine structure of the nervous system: the neurons and supporting cells. Philadelphia: Saunders.
- Raff MC, Miller RH, Noble M (1983) A glial progenitor cell that develops *in vitro* into an astrocyte or an oligodendrocyte depending on culture medium. *Nature* 303:390–396.
- Ransom BR, Butt AM, Black JA (1991) Ultrastructural identification of HRP-injected oligodendrocytes in the intact rat optic nerve. *Glia* 4:37–45.
- Sandell JH, Masland RH (1988) Photoconversion of some fluorescent markers to a diaminobenzidine product. *J Histochem Cytochem* 36:555–559.
- Skoff RP (1990) Gliogenesis in rat optic nerve: astrocytes are generated in a single wave before oligodendrocytes. *Dev Biol* 139:149–168.
- Skoff RP, Price DL, Stocks A (1976) Electron microscopic autoradiographic studies of gliogenesis in rat optic nerve. *J Comp Neurol* 169:291–312.
- Sontheimer H, Kettenmann H (1988) Heterogeneity of potassium currents in cultured oligodendrocytes. *Glia* 1:415–420.
- Sontheimer H, Trotter J, Schachner M, Kettenmann H (1989) Channel expression correlates with differentiation stage during the development of oligodendrocytes from their precursor cells in culture. *Neuron* 2:1135–1145.
- Sturrock RR (1975) A quantitative electron microscopic study of myelination in the anterior limb of the anterior commissure in the mouse brain. *J Anat* 119:67–75.
- Sturrock RR (1976) Light microscopic identification of immature glial cells in semithin sections of the developing mouse corpus callosum. *J Anat* 122:521–537.
- Sturrock RR (1980) Myelination of the mouse corpus callosum. *Neuropathol Appl Neurobiol* 6:415–420.
- Trotter J, Schachner M (1989) Cells positive for the O4 surface antigen isolated by cell sorting are able to differentiate into astrocytes or oligodendrocytes. *Dev Brain Res* 46:115–122.
- Vaughn JE, Peters A (1967) Electron microscopy of the early postnatal development of fibrous astrocytes. *Am J Anat* 121:131–152.
- Waxman SG, Sims TS (1984) Specificity in central myelination: evidence for local regulation of myelin thickness. *Brain Res* 292:179–185.